Computer Methods and Programs in Biomedicine 198 (2021) 105778

Contents lists available at ScienceDirect

Computer Methods and Programs in Biomedicine

journal homepage: www.elsevier.com/locate/cmpb

On the magnetic aggregation of Fe_3O_4 nanoparticles

E.G. Karvelas [a], N.K. Lampropoulos [b], L.T. Benos [c], T. Karakasidis [d,e], I.E. Sarris [a,*]

[a] Department of Mechanical Engineering, University of West Attica, Aigaleo, Greece
[b] Center for Renewable Energy Sources, Pikermi, Greece
[c] Institute for Bio-Economy and Agri-Technology (iBO), Centre for Research and Technology, Hellas (CERTH), Thessaloniki, Greece
[d] Department of Civil Engineering, University of Thessaly, Volos, Greece
[e] Department of Physics, University of Thessaly, Lamia, Greece

ARTICLE INFO

Article history:
Received 7 September 2020
Accepted 27 September 2020

Keywords:
Aggregations
Magnetic field
Computational fluid dynamics
Discrete element method
Nanoparticles

ABSTRACT

Background and objective *In-vivo* MRI-guided drug delivery concept is a personalized technique towards cancer treatment. A major bottleneck of this method, is the weak magnetic response of nanoparticles. A crucial improvement is the usage of paramagnetic nanoparticles aggregates since they can easier manipulated in human arteries than isolated particles. However its significance, not a comprehensive study to estimate the mean length and time to aggregate exists. *Methods* The present detailed numerical study includes all major discrete and continues forces and moments of the nanoscale in a global model. The effort is given in summarizing the effects of particle diameter and concentration, and magnetic field magnitude to comprehensive relations. Therefore, several cases with nanoparticles having various diameters and concentrations are simulated as magnetic field increases. *Results* It is found that aggregations with maximum length equal to $2000nm$ can be formed. In addition, the increase of the concentration leads to a decrease in the amount of the isolated particles. Consequently, 33% of the particles are isolated for the concentration of $2.25mg/ml$ while 13% for the concentration of $10mg/ml$. Moreover, the increase of the permanent magnetic field and diameter of particles gives rise to an asymptotic behavior in the number of isolated particles. Furthermore, the mean length of aggregates scales linear with diameter and magnetic field, however, concentration increase results in a weaker effect. The larger aggregation that is formed is composed by 21 particles. Smaller time is needed for the completion of the aggregation process with larger particles. Additionally, the increase of the magnitude of the magnetic field leads to a decrease in the aggregation time process. Therefore, $8.5ms$ are needed for the completion of the aggregation process for particles of $100nm$ at $B_0 = 0.1T$ while $7ms$ at $B_0 = 0.9T$. Surprisedly, the mean time to aggregate is of the same order as in microparticles, although, with an opposite trend. *Conclusions* In this study, the evolution of the mean length of aggregations as well as the completion time of the aggregation process in the nano and micro range is evaluated. The present results could be useful to improve the magnetic nanoparticles assisted drug delivery method in order to minimize the side effects from the convectional cancer treatments like radiation and chemotherapy.

1. Introduction

Cancer is a disease that is related to abnormal cell evolution. Conventional treatments involve surgery, chemotherapy and radiation, which use drugs and high doses of radiation, respectively, to shrink tumors. However, surgery is limited by its invasive nature, while radiotherapy suffers from the risk of necrosis and resistance of certain types of tumors. Moreover, chemotherapy results in severe side effects that include nausea, hair loss, nerve damage and infertility to mention but a few [1]. As a consequence, state-of-the-art personalized drug delivery targeted methods have been developed as a means to minimize side effects.

The most advanced concept of targeted therapy is achieved by drug delivery due to magnetic nanoparticles (MNPs) which are guided by external magnetic fields near tumors. In this drug delivery method, the surface of particles is coated by medicine [2] before injected into the blood flow of human body by a catheter. Consequently, particles can release the coated drug only in the tumor area, resulting in less chemical loads and avoiding its extensive spread in healthy cells compared to the classical chemotherapy [3]. For the navigation of magnetic nanoparticles towards the desired areas (tumors), strong magnetic fields may be needed due MNPs weak magnetic response [4,5]. These magnetic fields can be

* Corresponding author.
E-mail address: sarris@uniwa.gr (I.E. Sarris).

https://doi.org/10.1016/j.cmpb.2020.105778
0169-2607/

Nomenclature

u	Fluid velocity
m	mass
d_i	Diameter
$\boldsymbol{u}$	Transversal velocity
$\boldsymbol{\omega}$	Rotational velocity
t	time
$\boldsymbol{I}$	Mass moment of inertia matrix
$\boldsymbol{F_{mag}}$	Total magnetic force
$\boldsymbol{F_{nc}}$	Normal contact force
$\boldsymbol{F_{tc}}$	Tangential contact force
$\boldsymbol{F_{drag}}$	Hydrodynamic drag force
$\boldsymbol{F_{grav}}$	Gravity and buoyancy force
$\boldsymbol{F_{vdw}}$	Van der Walls force
$\boldsymbol{F_{br}}$	Brownian force
$\boldsymbol{F_{nc}}$	Scaled end-region fluid temperatures
$\boldsymbol{M_{drag}}$	Drag moment
$\boldsymbol{F_{con}}$	Contact moment
$\boldsymbol{T_{mag}}$	Torque due to magnetic field
$\boldsymbol{B_0}$	Permanent magnetic field (T)

Subscripts

mag	Magnetic
nc	Natural contact
tc	Tangential contact
grav	Gravity
con	Contact

created nowadays by a Magnetic Resonance Imaging (MRI) device. When nanoparticles are nearby tumors, drug transport due to *pH* fluctuations is initiated and medicine is driven due to the concentration difference to the affected cells [6]. Remarkably, magnetic fields in nanoparticles have also been implemented in cancer therapy via hyperthermia, which aims to the tumor death via local temperature increase in abnormal levels [7].

In recent years, nanoparticles have been the main subject of biomedical research since they present several advantages [8]. In brief, iron oxide nanoparticles were successfully used in the treatment of inflammatory joint diseases [9]. In addition, nanoparticles can be found in cellular labeling/cell separation, detoxification of biological fluids, tissue repair and magnetofection [10]. Furthermore, magnetic multifunction nanoparticles are used for cell targeting [7], targeting of selective tissue markers [11], chemical conjugation for targeted thrombolysis [12], non-invasively targeting respiratory tract deposition of high aspect ration aerosols [13] and many other biomedical applications.

Nanoparticles possess some attractive features: The high surface to volume ratio compared to conventional materials [14] and that their dimensions are smaller or comparable to those of a single cell ($10-100\ nm\ length$), virus ($20-450\ nm$), a protein ($5-50\ nm$) or a gene ($2\,nm$ width and $10-100\ nm$ length) [14,15]. The above features make them ideal candidates for biomedical applications, as they can be coated with biological molecules, that can lead to reacting or binding to a biological entity [16]. Moreover, nanoparticles can be paramagnetic i.e. to act like tiny magnets only when external magnetic fields are applied and demagnetized as soon as the field is turned off. Thus, they can be driven by an external magnetic field to desired areas through the blood stream, a concept that is illustrated in Fig. 1. Additionally, they can be affected by a radio frequency (RF) magnetic field to enable thermal energy transfer due to Joule heating [17–22]. On the other hand, the presence of nanoparticles inside the blood affects the fluid flow [23,24].

Magnetic nanoparticles have already been proposed as a promising alternative for drug delivery in biomedical applications for the treatment of cancer cells [15,25,26]. The efficiency of the magnetic guided drug delivery method is found to depend on several physical aspects [18,27,28]. Firstly, the core material of the magnetic particles and the coatings possess magnetic properties that may cause important differences in the driving [29]. In addition, the size of particles is a crucial parameter for the effectiveness of the method, since, the smaller the size of the particles the weaker their magnetic response will be. Consequently, increased difficulty in gradient magnetic fields to navigate nanoparticles into artery bifurcations may be observed. To overcome this difficulty, permanent fields are used with paramagnetic nanoparticles due to their ability to form clusters that can be easily separated close to the tumors. Clustering occurs since this kind of particles become magnets and might attract the nearby ones inside an interaction distance [30,31]. These clusters of particles are aligned along the magnetic field lines and can be more easily driven by gradient magnetic fields due to their higher magnetic volume than single particles [32]. Once the aggregations are driven close to the targeted area, they can split into single particles by switching off the magnetic field in order to facilitate the drug release [30]. As a consequence, the use of paramagnetic particles seems to be advantaged since no magnetic hysteresis is observed in this kind of materials [33]. Additional properties of magnetic nanoclusters include tunable cluster size, efficient drug loading, and enhanced drug uptake in cancer cells with no apparent decrease in the inherent magnetization characteristics [34].

The strength of the external magnetic field is the most important parameters in the aggregations process [35,36]. Weak magnetic fields result in weak dipole-dipole interactions between particles and thus can only create small aggregations [5]. Besides, gradient magnetic field can not drive small aggregations due to their weak total magnetic moment. On the other hand, very long aggregations could form clots in small arteries, especially when they pass through possible stenosis.

In a recent study [35], the effect of magnetic field magnitude and gradient in aggregates formation and motion has investigated in the range of magnetic microparticles. Those results helped us in establishing the methodology for the connection of crucial parameters towards the drug delivery method. This methodology is applied here by examining the more practical consideration pertaining to biomedicine, specifically the use of nanoparticles. It should be noted that there is a lack of studies in the field of the aggregation of paramagnetic nanoparticles under the action of the permanent magnetic field. Hence, at the present study, a numerical model for the nanoparticle aggregations formation, based on the OpenFOAM® platform, is further developed [37]. The size of nanoparticles and their concentration as well as the magnitude of the uniform magnetic field are numerically examined. It is the first time, at least to the authors knowledge, that such a numerical investigation is presented which, in conjunction with our recent study [35], covers the entire range of interest of particles that are used in biomedical applications, namely from nanometers to micrometers. Therefore, the parameters that mostly affect the aggregation process in the nano range are evaluated and compared with those in the micro range. This have a tremendous effect in the calculation of the gradient field for the magnetic navigation of particles in the desired areas. Better understanding of magnetic aggregation processes inside human body will lead to the identification of avenues for more effective and selective drug delivery; for example, effective magnetic navigation of drug-coated nanoparticles into targeted areas hinges on a quantitative understanding of the effect of the permanent magnetic field on paramagnetic particles, so that optimized quantities of drugs will be used for maximum benefit and minimal side effects. It should be noticed that the numerical method that is used in this study has been validated against experimental results that uses water as testing

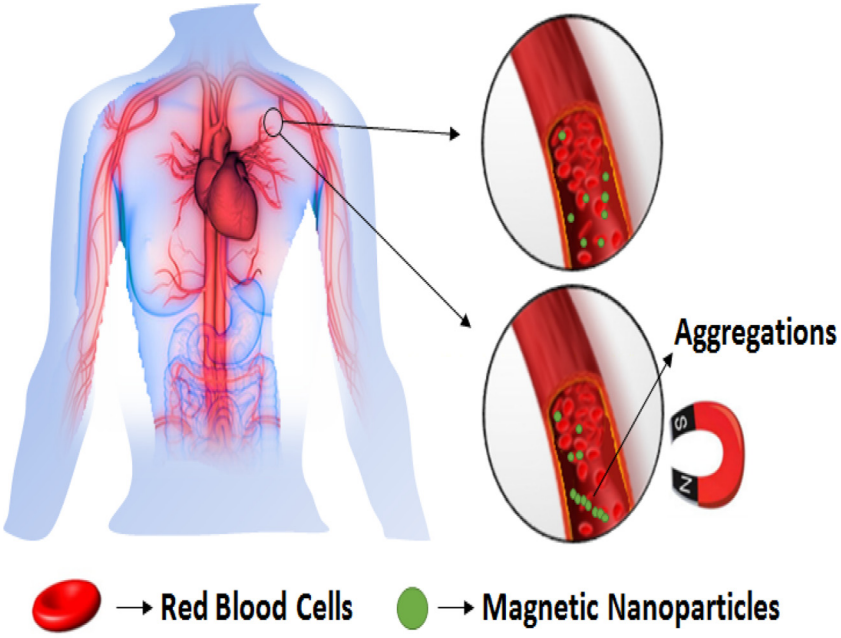

Fig. 1. Schematic representation of the magnetic navigation concept.

in-vitro fluid solutions [30,38]. Therefore, all the simulations in this study are conducted in such solutions. The governing equations and all important numerical details are presented in Section 2. Results concerning the mean length and the time to aggregate under various permanent magnetic field magnitudes are quantified in Section 3. Emphasis is also given in Section 4 to correlate data of nanoparticle and microparticle aggregates for various magnetic fields and concentrations. The most important conclusions are summarized in Section 5.

Table 1
Particles' and simulations conditions.

Property	*Units*
Particles' density	$5000\,Kg/m^3$
Young's modulus	$3.5 \cdot 10^9$ Pa
Poisson's ratio	0.34
Relative magnetic permeability	1.23
Medium permeability	$1.256 \cdot 10^{-6}$
Temperature	288 K
Molecular mean free path	$2.5 \cdot 10^{-9}$

2. Material and methods

The numerical model used in the present study is based on a successfully validated model regarding the motion of microparticles under uniform and gradient magnetic field in [35,39]. The present model is extent to include Van der Waals and Brownian forces due to the nanoscale of the particulate simulations [38,40]. An extensive description of all numerical details for our model can be found in Refs. [35,37] and only a brief description follows to avoid duplication of already published material.

The general purpose numerical library OpenFOAM® [41] is employed in three-dimensional domains, as a framework for the simulation of both fluid and particles flow in the suspension. The incompressible Navier-Stokes equations are solved for the Eulerian phase together with a Lagrangian model for the tracking of particles in the discrete phase [35]. In the present study, only simulations of fluid at rest are considered. Due to the small number of nanoparticles no coupling between the fluid and discrete phases is taken into consideration.

The discrete equations are based on the Newton's second law and for every particle may read as [42]:

$$m_i \frac{\partial \boldsymbol{u}_i}{\partial t} = \boldsymbol{F}_{mag,i} + \boldsymbol{F}_{nc,i} + \boldsymbol{F}_{tc,i} + \boldsymbol{F}_{drag,i} + \boldsymbol{F}_{grav,i} + \boldsymbol{F}_{wdv,i} + \boldsymbol{F}_{br,i} \quad (1)$$

$$\boldsymbol{I}_i \frac{\partial \boldsymbol{\omega}_i}{\partial t} = \boldsymbol{M}_{drag,i} + \boldsymbol{M}_{con,i} + \boldsymbol{T}_{mag,i} \quad (2)$$

where, the index i stands for the i^{th}-particle with diameter and mass noted by d_i and m_i, respectively. The mass moment of inertia matrix is $\boldsymbol{I}_i$ while t is time and $\boldsymbol{u}_i$, $\boldsymbol{\omega}_i$ are its transversal and rotational velocities, respectively. Terms $\frac{\partial \boldsymbol{u}_i}{\partial t}$ and $\frac{\partial \boldsymbol{\omega}_i}{\partial t}$ correspond to its linear and angular accelerations, respectively. $\boldsymbol{F}_{mag,i}$ is the total magnetic force, while $\boldsymbol{F}_{nc,i}$ and $\boldsymbol{F}_{tc,i}$ stands for the normal and tangential contact forces, respectively, $\boldsymbol{F}_{drag,i}$ and $\boldsymbol{F}_{grav,\,i}$ are the hydrodynamic drag and buoyancy forces, respectively, and $\boldsymbol{F}_{wdv,\,i}$ and $\boldsymbol{F}_{br,i}$ are the Van der Waals and Brownian forces, respectively. $\boldsymbol{M}_{drag,i}$ and $\boldsymbol{M}_{con,i}$ are drag and contact moments, respectively, and finally, $\boldsymbol{T}_{mag,i}$ is the magnetic torque at the position of particle i. All forces and moments are calculated according to Discrete Element Method (DEM) method as in [35].

The Lagrangian motion of 100 magnetically interconnected particles is evaluated by solving Eqs. (3) and (4) along with their trajectories. This particle number is considered reasonable in order vast the numerical load to remain resonable since the maximum number of MNPs aggregates is found to be 20 for the range of magnetic field used here. The implicit Euler method is incorporated for the time marching equations with a time step of $10^{-9}s$ that ensures the stability of the algorithm. The *MPI* technique is used for the effective communication across multiple processors in order to accelerate the simulations [41].

The physical material properties of particles and other important parameters used in this study are the same as in Ref. [38] and are summarized in Table 1. To avoid effects of the boundary condition in aggregation formation of the particles, all simulations are performed in a large cubic domain. The length of each edge of the cube is equal to $2.95 \cdot 10^{-6}$ m. The particles are initially randomly placed in the center of the computational domain in such a way to satisfy the requirements of each simulated concentration. An equi-

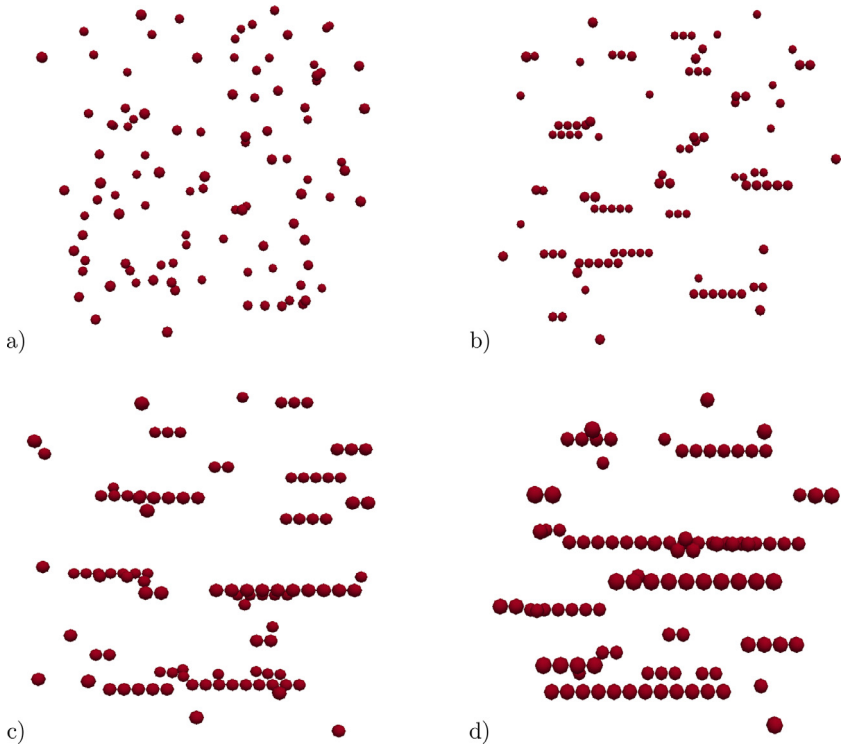

Fig. 2. Indicative initial particles random locations of diameter $D = 50\ nm$ (a) and aggregations formation for $B_0 = 0.5\ T$ for concentrations: b) $2.25\ mg/ml$, c) $4.5\ mg/ml$, and d) $10\ mg/ml$.

spaced computational grid is used in every direction with mesh size equal to the diameter of corresponding particles of each simulation.

3. Results and discussion

Spherical Fe_3O_4 nanoparticles of diameters 50, 75 and $100\ nm$ are examined in solutions of concentration 2.25, 4.5 and $10\ mg/mL$ for horizontal homogeneous magnetic field of magnitudes in the range 0 to $0.9\ T$. It should be noticed that no external gradient magnetic field is allowed during the present simulations, thus, only the aggregation formation is observed without any chains drift. Emphasis is given to the ability of the magnetic field to interconnect as much as possible of the nanoparticles in the aggregates and leave only a small of their fraction isolate.

Indicative snapshots of initial positions of nanoparticles and the formed aggregations after equilibrium are presented in Figs. 2 and 3 for different concentrations and diameters, respectively. More specifically, the concentration effect in aggregations consisting of particles with diameter of $50nm$ and for $B_0 = 0.5\ T$ is presented in Fig. 2. As particle concentration increases and their interparticle distances are getting smaller, the amount of isolated particles is found to decrease.

The aggregation process from the random initial stage to the equilibrium one for the indicative concentration of $4.5\ mg/mL$ and a magnetic field of magnitude $B_0 = 0.7\ T$ is presented in Fig. 3 in the diameter range studied here. We should notice that MNPs diameter increase results in increase of their volume and magnetic moment and thus, in their ability to attract other nearby particles. Substantially, larger nanoparticles are expected to form longer aggregates for similar concentration and magnetic field magnitude conditions. Therefore, in these particular cases of Fig. 3, 12 particles are contained in the larger aggregates of $50\ nm$ particles ($600\ nm$ total aggregation length), while 20 may be found in the larger aggregates of the case of $100\ nm$ nanoparticles ($2000\ nm$ total aggregation length). As we can see in Fig. 4, for the smaller concentration of $2.25\ mg/mL$, about 33% of particles are found to be isolated. The number of isolated particles decreases to about 21% for the concentration of $4.5\ mg/mL$ and to 13% for the higher concentration of $10\ mg/mL$. Consequently, although concentration, C, increases by a factor 4, the number of isolated particles decreases by a factor 2.53. This non-linear response to C is also observed for all particles diameters and magnetic field magnitudes, as it is shown in Fig. 4. Therefore, an asymptotic behavior of the isolated particles as the permanent magnetic field increases is observed. As a consequence, even with the higher magnetic field magnitude used here, a 5 to 10% of the nanoparticles will not be attracted by the existing aggregates. The size of particle appears to affect the number of isolated MNPs that observed in the solution. As the magnetic field increases and the strength to aggregate is increases, the number of the isolated particles is asymptotically decreased, as is depicted in Fig. 4. This decrease is sharper as the diameter of the particles increases.

The number of particles in aggregates for different diameters and concentrations for $B_0 = 0.9\ T$ is indicatively presented in Table 2 and Fig. 5. Results for the concentration of $2.25\ mg/mL$ with particle diameter $50\ nm$, respectively, show for example, that three aggregates of 9 particles length may be formed. Moreover, as concentration increases to $4.5\ mg/ml$, three aggregates of eleven particles are formed for particles of diameter $75\ nm$ and so on. The longer aggregate of twenty nanoparticles may be formed in the cases of $75nm$ and $100\ nm$ diameters for concentration 4.5 and $10\ mg/mL$, respectively. The maximum length of aggregates for a constant magnetic field, thus, depend on the initial random locations of nanoparticles rather that their diameters and concentrations.

The mean length of aggregations, $\bar{l}$, as the magnetic field magnitude increases for the concentration of $2.25\ mg/mL$ is depicted in Fig. 6 for all sizes of nanoparticles studied here. As the magnetic field, and thus the dipole-dipole force increase, the param-

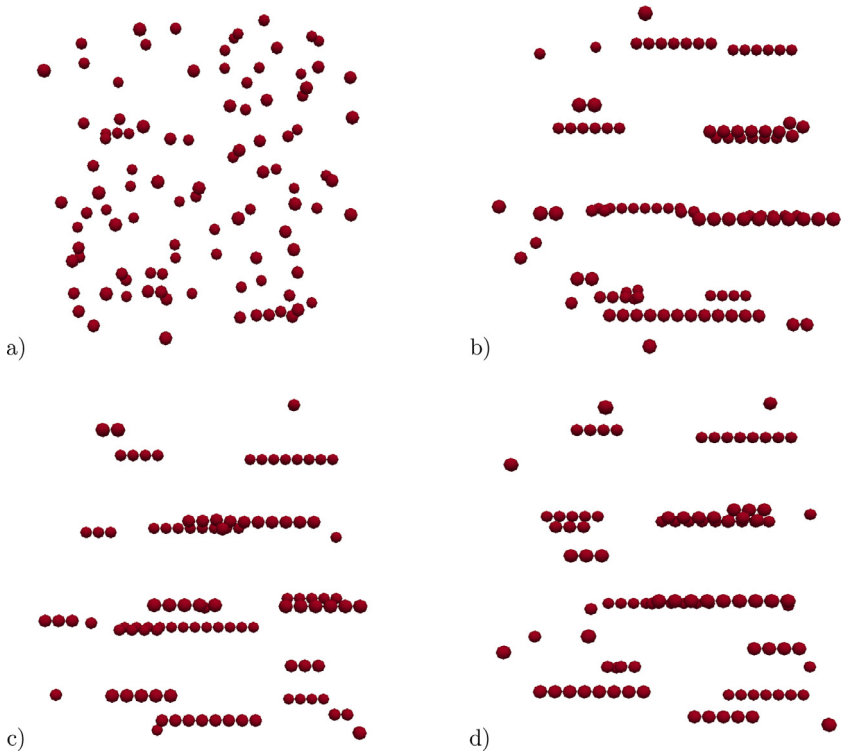

Fig. 3. Indicative initial particles random locations for $C = 4.5\ mg/mL$ (a) and aggregations formation for $B_0 = 0.7\ T$ (left) for diameters: b) $50\,nm$, c)$75\,nm$, and d) $100\,nm$.

Table 2
Number of MNPs in aggregates for $B_0 = 0.9T$ and various diameters and solution concentrations.

Diameter	50 *nm*			75 *nm*			100 *nm*		
	Concentration (*mg*/*mL*)								
# of Particles in aggregates	2.25	4.5	10	2.25	4.5	10	2.25	4.5	10
1	17	4	8	14	9	6	15	7	4
2	3	3	4	7	4	3	5	4	3
3	2	2	0	3	1	1	2	3	2
4	4	2	0	3	3	0	4	0	0
5	1	0	1	0	0	0	3	0	1
6	2	2	0	0	2	2	1	1	1
7	0	0	0	2	1	1	1	0	1
8	0	0	0	2	0	0	2	1	0
9	3	2	1	0	0	0	1	0	0
10	0	2	0	1	0	0	0	1	0
11	1	0	1	1	3	0	0	2	0
12	0	1	0	0	0	0	0	0	0
13	0	0	0	0	0	2	0	1	0
14	0	1	2	0	0	0	0	0	2
15	0	0	1	0	0	0	0	0	0
16	0	0	1	0	1	0	0	0	0
17	0	0	0	0	0	0	0	1	0
18	0	0	0	0	0	1	0	0	1
19	0	0	0	0	0	0	0	0	0
20	0	0	0	0	0	1	0	0	1

agnetic nanoparticles attract each other and the mean length of aggregates in the solution increases. A linear trend in this increase of $\bar{l}$ in cases with particles of 75 and $100\,nm$ is observed with B_0. It should be noticed that in cases of $50\,nm$ particles, an exponential trend in the increase of $\bar{l}$ is observed with B_0. It seems that for the lower concentration of $2.25\,mg/mL$, a maximum mean aggregation size of $450\,nm$ can be measured as a result of the relative higher particles distance from each other. Therefore, only a small fraction of particles can interact with others to form aggregates, even in the case of biggest nanoparticles.

As MNPs concentration increases from 2.25 to $4.5\,mg/mL$ a linear increase of the mean length of the aggregates for the cases of particles of 75 and $100\,nm$ is found. On the other hand, an exponential increase of $\bar{l}$ is observed in the case of $50\,nm$. Furthermore, an up to $\bar{l} \approx 700\ nm$ mean chain length may be measured in the solution for the largest simulated diameter of $100\,nm$, however, lessen than the double although the double concentration. As in the lower concentration case, $\bar{l}$ is shorter in the case of $75\,nm$, and even shorter for $50\,nm$ nanoparticles. Thus, as expected, only by increasing the magnetic field magnitude a significant increase of the mean length of aggregations is observed. Additionally, the

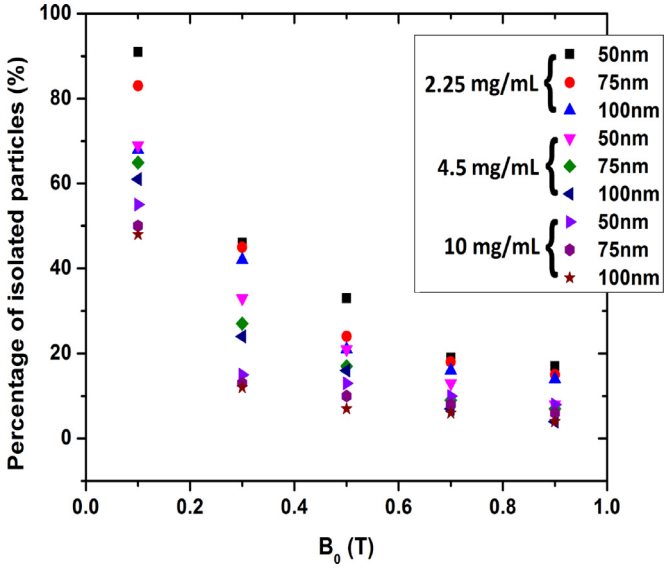

Fig. 4. Isolated particles rate (%) for various diameters and concentrations versus the magnitude of the magnetic field.

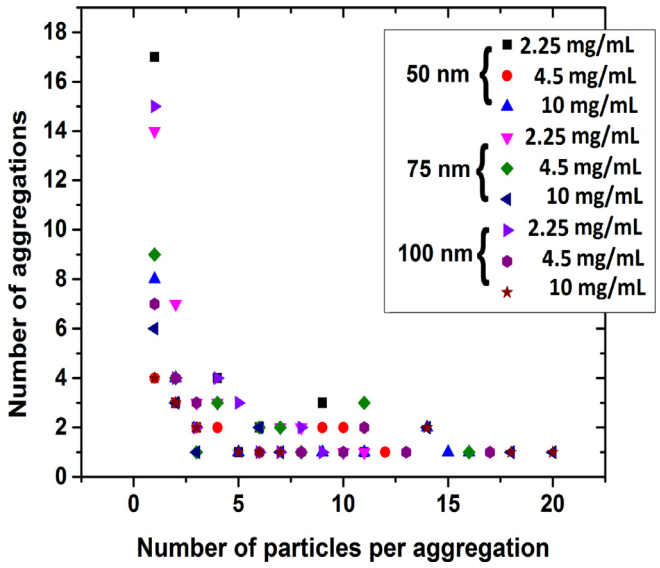

Fig. 5. Number of aggregates versus number of particles per aggregation for magnetic field magnitude of $B_0 = 0.9\ T$ and MNPs diameters of: a) $50\,nm$, b) $75\,nm$, and c) $100\,nm$.

mean length of aggregates for the smaller particles of $50\,nm$, seems to marginally be affected by the increase of B_0 for values lower than $0.5\,T$. In the case of $100\,nm$ MNPs, a similar effect is encountered for the lower concentration of $2.25\,mg/mL$. In the range of $0.3\,T \leq B_0 \leq 0.7\,T$, the same trend in $\bar{l}$ is also observed in the cases of 75 and $100\,nm$ particles. A steeper increase of $\bar{l}$ in aggregations of $100\,nm$ MNPs, compared to the cases of $75\,nm$ particles is observed for $B_0 = 0.9\ T$. The evolution of mean aggregates length with magnetic field magnitude for the $10\,mg/mL$ concentration solution is also illustrated in Fig. 6 for the different particle sizes. Although, a concentration of more than double than in the previous case is considered, only a small increase, from $\bar{l} \approx 700\ nm$ to approximately $750\,nm$ in the maximum mean aggregates length is noticed. Thus, it is found that solution concentration can only cause a secondary effect in the aggregation process.

From the above observations it turns out that the mean length of aggregates scales almost linear with the diameter and magnetic field magnitude and depends in a lessen extent by solution concentration. This is uniformly presented also in Fig. 7, where the dependence of $\bar{l}/D$ on B_0 may be expressed by:

$$\frac{\bar{l}}{D} \approx a_C B_0 + b_C \tag{3}$$

where, a_c and b_c are mostly concentration dependent quantities. It should be noticed that both a_C and b_C are monotonically increased with C as it is shown in Table 3. This occurs due to closer nanopar-

Table 3
Values of a_c and b_c in Eq. 3.

Concentration(mg/ml)	a_c	b_c
2.25	3.05	1.74
4.5	4.72	1.99
10	6.71	2.20

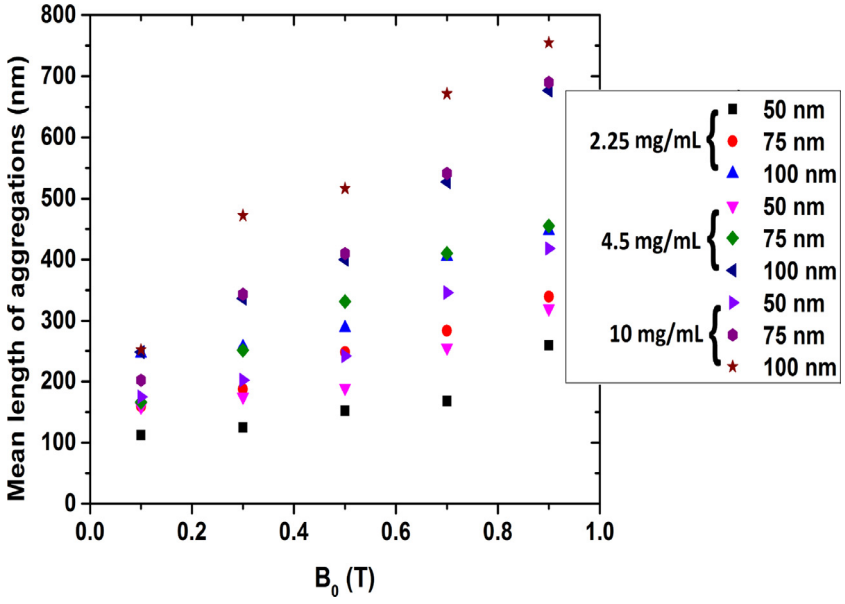

Fig. 6. Mean length of aggregations with the magnetic field magnitude for solution concentration of: a) $2.25\,mg/mL$, b) $4.5\,mg/mL$, and c) $10\,mg/mL$.

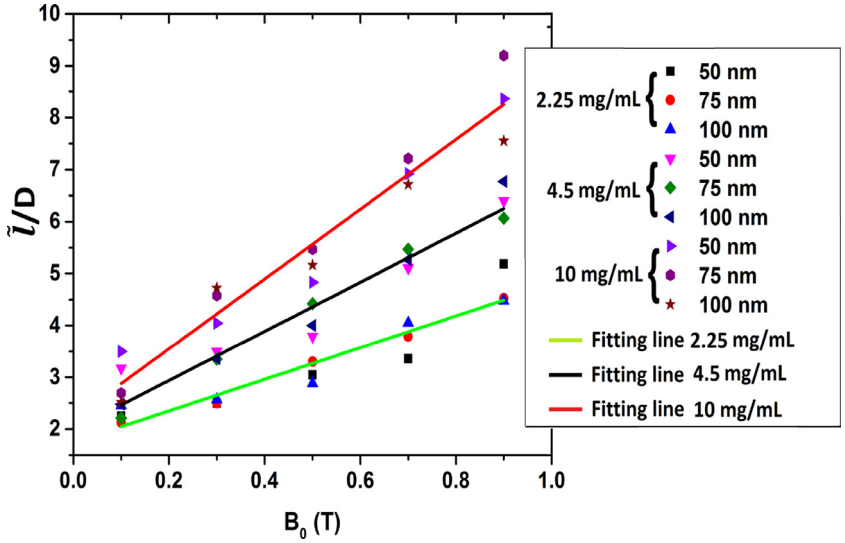

Fig. 7. Effect of magnetic field magnitude on $\bar{l}/D$ for concentrations 2.25 mg/ml, 4.5 mg/ml, and 10 mg/ml, with their least square fitting lines.

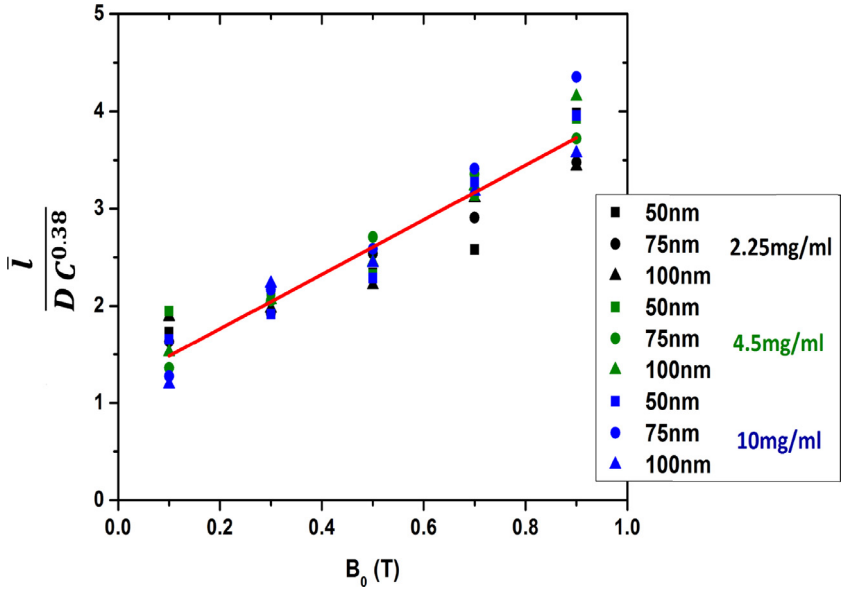

Fig. 8. Effect of magnetic field magnitude on $\bar{l}/DC^{0.38}$. Fitting least squares line (Red color).

ticles positions as concentration increases making it easier to interact and form aggregations. Thus, increase of concentration for every B_0 leads to a smother increase in mean length of aggregates that is found to approximately fit all C according to: $\bar{l} \approx B_0 DC^{0.38}$ as it is shown in Fig. 8.

Taking advantage of our simulations, it may be interesting to investigate differences in aggregations due to particles size as they vary from nanometers to micrometers. In our recent work [35], the mean length of aggregations for microparticles is found to approximately be scaled by $\bar{l}_m \approx B_0 D^{1.5}$ while here, the mean length of nanoparticles aggregates in the similar to [35] concentration of $2.25 mg/mL$ is found, after compiling all our data, to scale according to the relation: $\bar{l} = D{B_0}^{0.32}$ as it is shown in Fig. 9. It should be noticed that both aggregates mean length distributions are measured at the same B_0 magnitude range, while the effects due to Brownian and Van der Waals forces are insignificant in the micrometer scale [43]. Differences in aggregations between the particle sizes occur also due the decreasing role of dipole-dipole magnetic interactions as the diameter of particles is decreased [38]. While mean aggregate chains of only ≈ 20 nanoparticles are formed even for a 10 mg/ml concentration solution and for $B_0 = 0.9\ T$, very longer chains of 50 or even 73 microparticles of size 11 μm may be measured for less than the half concentration at the same B_0.

In the low B_0 regime, Brownian and Van der Waals forces are found to play significant role in the motion of nanoparticles, and while the Brownian motion is of random nature [44], dipole-dipole force is proportional to the magnetic moments of particles [45]. Therefore, it is likely that Brownian motion opposites to aggregation process, while dipole-dipole and Van der Waals forces helping it. As B_0 increases and interparticle magnetic interactions are enhanced, the effect of Brownian motion in aggregation process decreases. In addition, for concentrations of 2.25 and 4.5 mg/ml the mean number of nanoparticles in aggregations is approximately 12.76 and 26.2, respectively. In the case of the larger nanoparticles of $100nm$, the mean number of particles is approximately 3.5 for both concentrations. This indicates that the size of particles compensates the magnetic attraction from other particles. In microme-

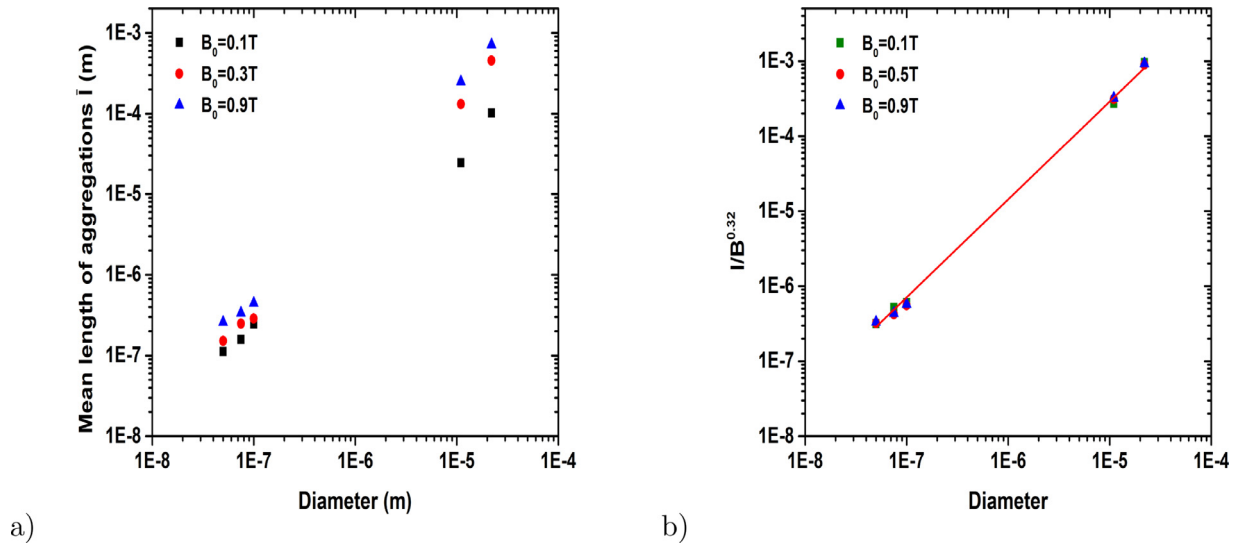

Fig. 9. Mean aggregation length versus particle diameter (a) and scaled also by $\bar{l}/(B_0)^{0.32}$ (b). Fitting line (red color).

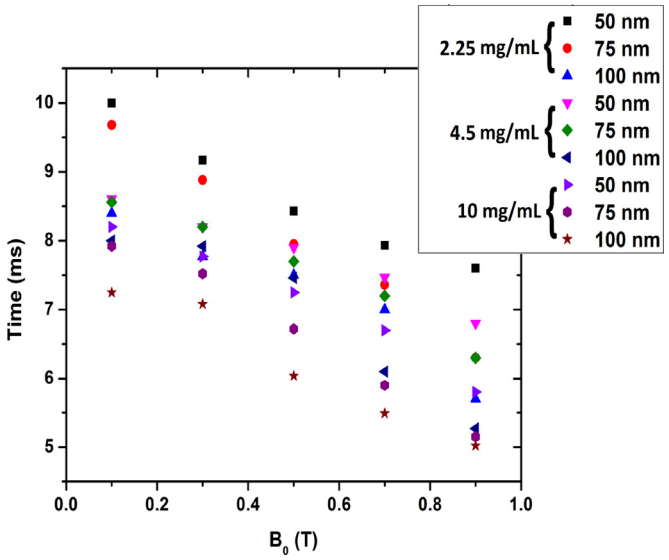

Fig. 10. Aggregation process duration against the magnetic field magnitude for the various solution concentrations and MNPs diameters.

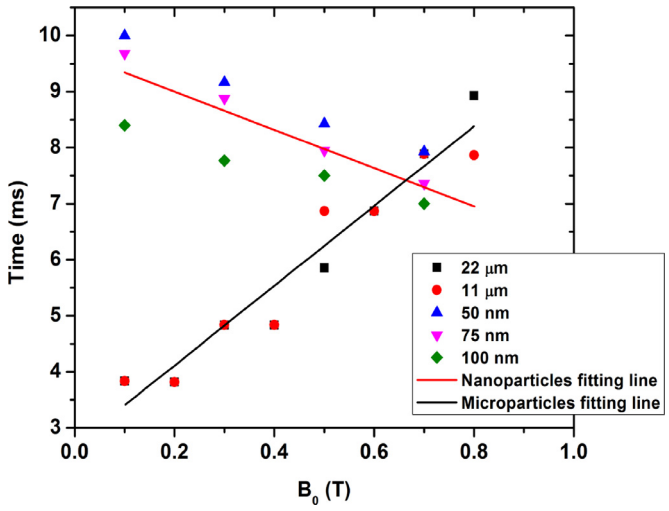

Fig. 11. Mean aggregation time for microparticles (black fitting line) [35] and nanoparticles for (red line) concentration of 2.25*mg/mL* versus the magnetic field magnitude.

ter scale, the mean particle number in the aggregates is more than doubled with the increase of concentration from 2.25 to 4.5 *mg/ml*.

Another important result of the present study is the aggregation process duration prediction. It should be noticed that aggregates are formed faster as the magnetic field magnitude increases as it is shown in Fig. 10. An indicative time needed for the aggregation process at $B_0 = 0.1\ T$, $C = 2.25\ mg/ml$ and $75\ nm$ size to complete is about $9.7\ ms$. As B_0 increases to $0.9\ T$, aggregation time is reduced to $6.3\ ms$ in the same case. Further increase of particle's size reduces further the process duration due to enhanced magnetic interactions among bigger particles (with larger magnetic moments) [38]. This effect is more pronounced in the lower concentration case where the size increase from $50\ nm$ to $100\ nm$ shortens further the aggregation duration to approximately $2.5\ ms$ (i.e about 25%). As concentration increases, aggregation duration decrease is about $1.5 - 2\ ms$ for $4.5\ mg/ml$ and approximately $1\ ms$ for $10\ mg/ml$. This is because of the smaller interparticle distance as solution concentration increases [30]. For $B_0 = 0.9\ T$ and size $100\ nm$, only $5\ ms$ are needed for the aggregations to be fully formed for the concentration of $10\ mg/ml$ (Fig. 10c). The time increases to about $5.27\ ms$ and $5.7\ ms$ for concentrations of 4.5 and $2.25\ mg/ml$ as it is depicted in Fig. 10.

Thus, it appears here that the duration of the aggregation process scales unexpectedly oppositively in nanoparticles than in microparticles. This different slope of mean time to aggregate can be seen in Fig. 11 for both kinds of particles and can be described by $\bar{t} \approx -3.5B_0$ for nanoparticles and $\bar{t} \approx 7B_0$ for microparticles [35]. Consequently, microparticles may need more time to aggregate than nanoparticles for $B_0 > 0.65$, while aggregates faster for $B_0 < 0.65$. Despite this opposite slope, as can be easily seen from Fig. 11, the mean aggregation duration is of the same order for the two kind of particles. This can be attributed to the increased magnetic interaction distance of microparticles that gives them the ability to attract other particles from far away, something that is slow, and also to the increased chains length of the microparticle aggregates [35]. On the other hand, short nanoparticle aggregates may be formed faster although their small magnetic moment, due to the shorter attraction range [31] and smaller re-

sponse time of nanoparticles with the increase of the permanent magnetic field [46].

Magnetic nanoparticles can safely be used for biomedical applications if the properties of nanomaterials remain unchanged. It is known that the degradation products of Fe_3O_4 nanoparticles that are occurring during the biotransformation can be included in iron metabolic routes of the organs [47–49]. On the other hand, the existence of salts and proteins in the human vascular system and the nanoparticle synthesis leads to materials with different properties. Thus, this can further alter the *in vivo* aggregation process of nanoparticles. In addition, differences in properties of the materials could also affect the biocompatibility of the magnetic nanoparticles. A small proportion of nanoparticles are degraded in cells while the rest particles maintain their size. This is caused due to the activation of genes which are involved in iron metabolism in macrophage cultures and the increased ferritin expression.

In our study, all of the simulations are conducted in water solutions. It should be noted that particles interactions are stronger in some organs than in water solutions [50]. Therefore, the mean length of the aggregations may be longer inside the human organs. In addition, the increase in the dipole-dipole interaction, with the increase of the magnitude of the magnetic field, decreases the *SAR* of the Fe_3O_4 due to the minimizing of the average distance among nanoparticles [51,52]. Therefore, the aggregations of the nanoparticles are not preferred when magnetic hyperthermia method is used as a cancer treatment technique. In order to prevent the agglomeration of the nanoparticles, special coating is used on their surface area [53]. On the other hand, the increase of the dipole-dipole interactions among the nanoparticles leads to aggregations with increased length. These aggregations give rise to enhanced magnetism [54] which is preferred in the magnetic navigation of nanoparticles method. The magnetic volume of an aggregation is bigger than that of an isolated particle. Therefore, the aggregations can easier br manipulated by the magnetic field [30].

4. Conclusions

In this study, Fe_3O_4 nanoparticles are considered for a range of concentrations, particle sizes, magnetic field magnitudes, while their mean length and time to aggregate are measured. Two important aspects are initially studied: under which conditions nanoparticles may stay isolated or may aggregate. Isolated particles are very difficult to be functionalized for drug delivery due to their weak magnetic response. Thus, from the initial particle population a 5 to even 50% of nanoparticles may be useless depending mainly on the magnetic field strength. Furthermore, the mean length and the mean time to aggregate is found to vary according to $\bar{l} \approx B_0 DC^{0.38}$ and $\bar{t} \approx -3.5B_0$, respectively.

The analysis is extended to cover a particle range from nanometers to micrometers under similar concentration and magnetic field conditions. To this end, our recent results [35] are exploited in order to generalize the aggregation process. From these data compilation, the mean length of aggregates is found to follow the relation $\bar{l} = DB_0{}^{0.32}$ universally from nano- to microscale. However, mean aggregation time is found to be of the same order for nano- and microparticles and to follow a different trend. In the case of nanoparticles $\bar{t}$ is minimized as the magnetic field increases while is growing in the case of microparticles.

The present results are anticipated to be of particular importance considering the ever increasing interest in magnetic nanoparticles navigation for drug delivery. The effect of the permanent magnetic field in the aggregation process under different size of particles and concentration is evaluated in this study. Based on the results of the present study, the calculation of the gradient magnetic fields as well as the imposed time of particles for a specific magnetic navigation towards to tumor cells is easier since the length of the aggregations is has been verified.

Acknowlgedgments

The authors would like to acknowledge the support of the Greek Research and Technology Network (GRNET) for the computational time granted in the National HPC facility ARIS.

References

[1] J.M. Torrisi, et al., CT findings of chemotherapy-induced toxicity: what radiologists need to know about the clinical and radiologic manifestations of chemotherapy toxicity, Radiology 258 (2011) 41–56.
[2] S. Murthy, Nanoparticles in modern medicine: state of the art and future challenges, Int. J. Nanomedicine 2 (2007) 129–141.
[3] W.H. De Jong, P.J. Borm, Drug delivery and nanoparticles: applications and hazards, Int. J. Nanomedicine 3 (2008) 133–149.
[4] A. Senyei, K. Widder, C. Czerlinski, Magnetic guidance of drug carrying microspheres, Appl. phys. 49 (1978) 3578–3583.
[5] K. Widder, P. Marino, R. Morris, A. Senyei, Targeted Drugs, Goldberg, New York, 1983.
[6] S.E. Samioti, L.T. Benos, I.E. Sarris, Effect of fractal-shaped outer boundary of glioblastoma multiforme on drug delivery, Comput. Method. Program. Biomed. 178 (2019) 191–199.
[7] A. Ito, M. Shinkai, H. Honda, T. Kobayashi, Medical application of functionalized magnetic nanoparticles, J. Biosci. Bioeng. 100 (2005) 1–11.
[8] T.K. Indira, P.K. Lakshmi, Magnetic nanoparticles - a review, Int. J. Pharmaceut. Sci. Nanotechnol. 3 (2010) 1035–1042.
[9] K. Schulze, et al., Intraarticular application of superparamagnetic nanoparticles and their uptake by synovial membrane-an experimental study in sheep, J. Magn. Magn. Mater 293 (2005) 419–432.
[10] A.L. Gupta, M. Gupta, Synthesis and surface engineering of iron oxide nanoparticles for biomedical applications, Biomaterials 26 (2005) 3995–4021.
[11] G. Huang, J. Diakur, Z. Xu, L.I. Wiebe, Asialoglycoprotein receptor-targeted superparamagnetic iron oxide nanoparticles, Int. J. Pharm. 360 (2008) 197–203.
[12] F. Bi, J. Zhang, Y. Su, Y. Tang, J. Liu, Chemical conjugation of urokinase to magnetic nanoparticles for targeted thrombolysis, Biomaterials 30 (2009) 5125–5130.
[13] A.R. Martin, W.H. Finlay, Enhanced deposition of high aspect ratio aerosols in small airway bifurcations using magnetic field alignment, J. Aerosci. 39 (2008) 679–690.
[14] M. Soloviev, Nanoparticles in Biology and Medicine: Methods and Protocols, Second ed., Springer, 2012.
[15] O.V. Salata, Applications of nanoparticles in biology and medicine, J Nanobiotechnol. 2 (2004).
[16] E. Blanco, H. Shen, M. Ferrari, Principles of nanoparticle design for overcoming biological barriers to drug delivery, Nat. Biotechnol. 33 (2015) 651–941.
[17] D.W.I. Rouson, S. Kassinos, I. Moulitsas, I.E. Sarris, X. Xu, Dispersed-phase structural anisotropy in homogeneous magnetohydrodynamic turbulence at low magnetic reynolds number, Phys. Fluid. 20 (2008) 25101–25119.
[18] Q.A. Pankhurst, J. Connoly, S.K. Jones, J. Dobson, Applications of magnetic nanoparticles in biomedicine, J. Phys. D 36 (2003) 167–181.
[19] R. Mohamed, F. Mabood, Entropy analysis of a hydromagnetic micropolar dusty carbon NTs-kerosene nanofluid with heat generation: Darcy–Forchheimer scheme, J. Therm. Anal. Calorim. (2020), doi:10.1007/s10973-020-09928-w.
[20] H. Berrehal, F. Mabood, O.D. Makinde, Entropy-optimized radiating water/FCNTs nanofluid boundary-layer flow with convective condition, Eur. Phys. J. Plus 135 (535) (2020), doi:10.1140/epjp/s13360-020-00536-z.
[21] F. Mabood, T.A. Yusuf, W.A. Khan, Cu-al2o3-h2o hybrid nanofluid flow with melting heat transfer, irreversibility analysis and nonlinear thermal radiation, J. Therm. Anal. Calorim. (2020), doi:10.1007/s10973-020-09720-w.
[22] A.K. Rostami, K. Hosseinzadeh, D.D. Ganji, Hydrothermal analysis of ethylene glycol nanofluid in a porous enclosure with complex snowflake shaped inner wall, Wave. Random Complex Media (2020), doi:10.1080/17455030.2020.1758358.
[23] K. Hosseinzadeh, S. Roghani, A.R. Mogharrebi, A. Asadi, M. Waqas, D.D. Ganji, Investigation of cross-fluid flow containing motile gyrotactic microorganisms and nanoparticles over a three-dimensional cylinder, Alex. Eng. J. (2020), doi:10.1016/j.aej.2020.04.037.
[24] K. Hosseinzadeh, A. Asadi, A.R. Mogharrebi, et al., Investigation of mixture fluid suspended by hybrid nanoparticles over vertical cylinder by considering shape factor effect, J. Therm. Anal. Calorim. (2020), doi:10.1007/s10973-020-09347-x.
[25] Y. Pathak, D. Thassu, Drug Delivery Nanoparticles Formulation and Characterization, CRC Press, London, 2009.
[26] L.E. Strong, J. West, Hydrogel-coated near infrared absorbing nanoshells as light- responsive drug delivery vehicles, Sci. Eng. 1 (2015) 685–692.
[27] M. Ramezanpour, et al., Computational and experimental approaches for investigating nanoparticle-based drug delivery systems, Biochimica et Biophysica Acta 1858 (2016) 1688–1709.
[28] V.P. Podduturi, I.B. Magana, D.P. O'Neal, P.A. Derosa, Simulation of transport and extravasation of nanoparticles in tumors which exhibit enhanced permeability and retention effect, Comput. Method. Program. Biomed. 112 (2013) 58–68.

[29] J. Llandro, J.J. Palfreyman, A. Ionescu, C.H.W. Barnes, Magnetic biosensor technologies for medical applications: a review, Med. Biol. Eng. Comput. 48 (2010) 977–998.
[30] J.B. Mathieu, S. Martel, Aggregation of magnetic microparticles in the context of targeted therapies actuated by a magnetic resonance imaging system, J. Appl. Phys. 106 (2009) 044904–044907.
[31] N.K. Lampropoulos, E.G. Karvelas, I.E. Sarris, Computational study of the particles interaction distance under the influence of steady magnetic field, Advan. Syst. Sci. Applic. 15 (2015) 233–241.
[32] P. Babinec, A. Krafcik, M. Babincova, J. Rosenecker, Dynamics of magnetic particles in cylindrical halbach array: implications for magnetic cell separation and drug targeting, Med. Biol. Eng. Comput. 48 (2010) 745–753.
[33] D. Jiles, Introduction to Magnetism and Magnetic Materials, Taylor & Francis, New York, 2010.
[34] D.H. Nquyen, et al., Hierarchical self-assembly of magnetic nanoclusters for theranostics: tunable size, enhanced magnetic resonance imagability, and controlled and targeted drug delivery, Acta Biomater 35 (2016) 109–117.
[35] E.G. Karvelas, N.K. Lampropoulos, I.E. Sarris, A numerical model for aggregations formation and magnetic driving of spherical particles based on openfoam®, Comput. Method. Program. Biomed. 142 (2017) 21–30.
[36] L.T. Benos, E.G. Karvelas, I.E. Sarris, Crucial effect of aggregations in CNT-water nanofluid magnetohydrodynamic natural convection, Therm. Sci. Eng. Progr. 11 (2019) 263–271.
[37] E.G. Karvelas, T.E. Karakasidis, I.E. Sarris, Computational analysis of paramagnetic spherical fe_3o_4 nanoparticles under permanent magnetic fields, Comput. Mater. Sci. 154 (2018) 464–471.
[38] P. Vartholomeos, C. Mavroidis, In silico studies of magnetic microparticle aggregations in fluid environments for MRI-guided drug delivery, Trans. Biomed. Eng. 59 (2012) 3028–3038.
[39] N.K. Lampropoulos, E.G. Karvelas, I.E. Sarris, Computational modeling of an MRI guided drug delivery system based on magnetic nanoparticle aggregations for the navigation of paramagnetic nanocapsules, in: 11th World Congress on Computational Mechanics, 5th European Conference on Computational Mechanics and 6th European Conference on Computational Fluid Dynamics, 2014, pp. 823–847.
[40] A. Li, G. Ahmadi, Dispersion and deposition of spherical particles from point sources in a turbulent channel flow, Aerosol. Sci. Technol. 16 (1992) 209–226.
[41] H.G. Weller, G. Tabor, H. Jasak, C. Fureb, A tensorial approach to computational continuum mechanics using object-oriented techniques, Comput. Phys. 12 (2010) 620–631.
[42] K. Iwashita, M. Oda, Mechanics of granular materials, An Introd. Lond. (1999).
[43] S.C. Glotzer, M.J. Solomon, N.A. Kotov, Self-assembly ; from nanoscale to microscale colloids, AIChE 50 (2004) 2978–2985.
[44] I. Koh, L. Josephson, Magnetic nanoparticle sensors, Sensors 9 (2009) 8130–8145.
[45] D. Jiles, Introduction to Magnetism and Magnetic Materials, Taylor & Francis/CRC, New York, 1998.
[46] H. Singh, P.E. Laibinis, T. A. Hatton, Rigid, superparamagnetic chains of permanently linked beads coated with magnetic nanoparticles. synthesis and rotational dynamics under applied magnetic fields, Langmuir 21 (2005) 11500–11509.
[47] A. Balakumaran, et al., Superparamagnetic iron oxide nanoparticles labeling of bone marrow stromal (mesenchymal) cells does not affect their "stemness", PLoS One 5 (7) (2010) e11462.
[48] M.C. Hohnholt, M. Geppert, R. Dringen, Treatment with iron oxide nanoparticles induces ferritin synthesis but not oxidative stress in oligodendroglial cells, Acta Biomater. 7 (11) (2011) 3946–3954.
[49] F. Mazuel, et al., Massive intracellular biodegradation of iron oxide nanoparticles evidenced magnetically at single-endosome and tissue levels, ACS Nano 10 (8) (2016) 7627–7638.
[50] J.M. Rojas, et al., Time-course assessment of the aggregation and metabolization of magnetic nanoparticles, Acta Biomaterialia 58 (2017) 181–195.
[51] N.A. Usov, O.N. Servebryakova, V.P. Tarasov, Interaction effects in assembly of magnetic nanoparticles, Nanoscale Res. Lett. 12 (2017) 489, doi:10.1186/s11671-017-2263-x.
[52] J.G. Ovejero, et al., Effects of inter- and intra-aggregate magnetic dipolar interactions on the magnetic heating efficiency of iron oxide nanoparticles, Phys. Chem. Chem. Phys. 18 (16) (2016) 10954–10963.
[53] N. Perez, et al., Aggregation state and magnetic properties of magnetite nanoparticles controlled by an optimized silica coating, J. Appl. Phys. 121 (2017) 044304.
[54] C. Jiang, C.W. Leung, P.W.T. Pong, Magnetic-field-assisted assembly of anisotropic superstructures by iron oxide nanoparticles and their enhanced magnetism, Nanoscale Res. Lett. 11 (2016) 189, doi:10.1186/s11671-016-1406-9.